

Micromachined silicon parallel acoustic delay lines as time-delayed ultrasound detector array for real-time photoacoustic tomography

This content has been downloaded from IOPscience. Please scroll down to see the full text.

2016 J. Opt. 18 024003

(<http://iopscience.iop.org/2040-8986/18/2/024003>)

View [the table of contents for this issue](#), or go to the [journal homepage](#) for more

Download details:

IP Address: 128.252.20.193

This content was downloaded on 11/02/2016 at 21:44

Please note that [terms and conditions apply](#).

Micromachined silicon parallel acoustic delay lines as time-delayed ultrasound detector array for real-time photoacoustic tomography

Y Cho¹, C-C Chang¹, L V Wang² and J Zou¹

¹Texas A&M University, Department of Electrical and Computer Engineering, College Station, TX 77843, USA

²Washington University in St. Louis, Department of Biomedical Engineering, St. Louis, MO 63130, USA

E-mail: junzou@ece.tamu.edu

Received 25 September 2015, revised 13 November 2015

Accepted for publication 18 November 2015

Published 6 January 2016



CrossMark

Abstract

This paper reports the development of a new 16-channel parallel acoustic delay line (PADL) array for real-time photoacoustic tomography (PAT). The PADLs were directly fabricated from single-crystalline silicon substrates using deep reactive ion etching. Compared with other acoustic delay lines (e.g., optical fibers), the micromachined silicon PADLs offer higher acoustic transmission efficiency, smaller form factor, easier assembly, and mass production capability. To demonstrate its real-time photoacoustic imaging capability, the silicon PADL array was interfaced with one single-element ultrasonic transducer followed by one channel of data acquisition electronics to receive 16 channels of photoacoustic signals simultaneously. A PAT image of an optically-absorbing target embedded in an optically-scattering phantom was reconstructed, which matched well with the actual size of the imaged target. Because the silicon PADL array allows a signal-to-channel reduction ratio of 16:1, it could significantly simplify the design and construction of ultrasonic receivers for real-time PAT.

Keywords: handheld probe, laser micro-machining, microfabrication, photoacoustic tomography, ultrasonic imaging, real time, single-crystalline silicon

(Some figures may appear in colour only in the online journal)

1. Introduction

In biooptics, high-resolution optical imaging modalities, such as confocal microscopy [1], two-photon microscopy [2], and optical coherence microscopy [3], have played a very important role. However, their imaging resolution can be maintained only within a shallow depth (e.g., <1 mm) due to the strong light scattering in biological tissues [4, 5]. In recent years, photoacoustic imaging has emerged as a fast growing hybrid imaging modality to break through the fundamental limitation of imaging depth. It is based on the detection of the photoacoustic (PA) waves induced by pulsed laser or electromagnetic waves. It combines the advantages of optical and ultrasonic imaging, and can provide high optical

absorption contrast and deep ultrasonic penetration depth [6–8]. Based on its actual implementation [9], photoacoustic imaging can be divided into photoacoustic microscopy (PAM) and photoacoustic tomography (PAT). PAM uses a (focused) single-element ultrasound transducer to detect PA signals pixel-by-pixel with mechanical or optical scanning [10]. PAT utilizes an ultrasound array system (1D or 2D) to detect multiple PA signals simultaneously without mechanical scanning. 2D or 3D PA images can be reconstructed based on a number of algorithms [11–13]. However, the construction of ultrasound receiving systems becomes more complicated and costly as the number of ultrasound transducer elements and data acquisition (DAQ) channels increases. To address this issue, we have demonstrated a handheld probe which

consisted of two arrays of parallel acoustic delay lines (PADLs) made of tightly wound fused-silica optical fiber coils [14]. Each optical-fiber PADL array can transmit eight channels of PA signals from the imaging target to a single-element ultrasonic transducer, while imposing a different acoustic time delay on each PA signal. As a result, the eight time-delayed PA signals will reach a single-element ultrasonic transducer at different times and therefore can be received unmixed. With this probe, PAT was successfully conducted by collecting and reconstructing 16 channels of PA signals using only two ultrasonic transducers and two DAQ channels, which corresponds to a signal-to-channel reduction ratio of 8:1. However, although they can transmit ultrasound signals, fused-silica optical fibers are not ideal materials for constructing the PADLs. First, they are very stiff and brittle, and therefore are difficult to be tightly wound into compact coils. Second, the protective polymer jacket layer can cause acoustic attenuation and distortion especially for higher-frequency signals. Third, once they are fabricated, mechanical supporting structures are needed to hold the optical-fiber PADLs in place. However, additional acoustic loss and coupling could occur at the contacts between the optical fibers and the supporting structures. These factors limited the number of the PADLs that could be practically built and used, and therefore the signal-to-channel reduction ratio and field of view of the PAT probe.

In this paper, we report the development of a new micromachined silicon PADL array [15] and the initial demonstration of its application in real-time PAT. As an almost perfectly elastic crystal material, single-crystalline silicon is a mechanically strong material, which also has extremely low acoustic attenuation even in the MHz range [16]. Complex microstructures can be directly fabricated on a silicon substrate in one step by using photolithography and deep reactive ion etching (DRIE). Therefore, single-crystalline silicon is structurally superior to optical fibers for the construction of PADLs. In this work, a 16-channel silicon PADL array was developed and its application for real-time PAT was demonstrated. The silicon PADL array was interfaced with one single-element transducer followed by one channel of DAQ electronics to receive 16 channels of PA signals simultaneously. It allowed a signal-to-channel reduction ratio of 16:1, two times higher than that of the optical fiber PADL array demonstrated previously [14, 17]. Therefore, this new acoustic time delay approach could further simplify the design and construction of ultrasonic receivers for real-time PAT.

2. Design and construction

2.1. Design

Due to the high acoustic velocity ($\sim 8430 \text{ m s}^{-1}$ [18]) of silicon, an acoustic delay length ranging from a few to tens of centimeters is necessary to provide suitable acoustic time delays (1–10 μs) between two adjacent PADLs, so that the PA signals do not overlap with each other and therefore can

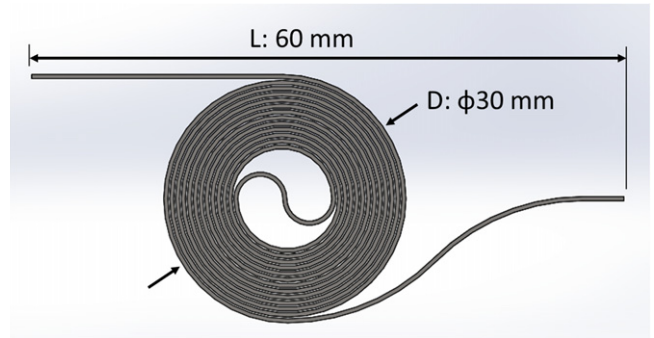


Figure 1. Schematic design of the longest (16th) silicon PADL.

Table 1. Main design parameters of silicon PADLs.

Parameter	Value
Number of channels	16
Shortest delay	9.5 μs
Longest delay	107 μs
Incremental delay	6.5 μs
Center frequency	2.25 MHz
Cross section	500 $\mu\text{m} \times 250 \mu\text{m}$
Minimum radius of curvature	2 mm

be clearly distinguished when they reach the single-element transducer [19]. To achieve a compact structure, the PADLs were designed as tightly wound spiral coils.

Figure 1 shows the schematic design of the longest (the 16th) PADL. The diameter of its circular portion is 30 mm, which is still compact even though its delay length reaches 90 cm. All 16 PADLs have the same span of 60 mm between their input and output terminals (L in figure 1), which facilitates the assembly and ease of contact between the imaging target and the single-element transducer.

Table 1 lists the main design parameters of the silicon PADL array. The shortest and longest acoustic time delays are 9.5 μs and 107 μs , respectively. The nominal incremental acoustic time delay between any two adjacent channels is 6.5 μs , which corresponds to a penetration depth of ~ 1 cm in soft tissue (assuming an acoustic velocity of $\sim 1500 \text{ m s}^{-1}$). The cross sectional area of the silicon PADLs is 500 $\mu\text{m} \times 250 \mu\text{m}$, which provides good mechanical stiffness (and therefore structural stability) and also good acoustic signal transmission for PA signals. For a rectangular acoustic delay line, its width or thickness (d) (whichever is smaller) should satisfy $(df/V_0) \ll 1$ to avoid signal distortion due to higher-order mode propagation and mode dispersion, where f is the frequency of the signal, and V_0 is the acoustic velocity of the delay-line material [20]. Assuming the silicon PADLs are interfaced with a single-element ultrasonic transducer with a center frequency of 2.25 MHz and a bandwidth of 100%, the maximum detection frequency will be 3.375 MHz. This value yields a df/V_0 ratio of 0.1 ($\ll 1$) to ensure single-mode transmission of the PA signals with minimal mode dispersion. Based on our previous simulation and experimental characterization results [19], the smallest radius of curvature in the

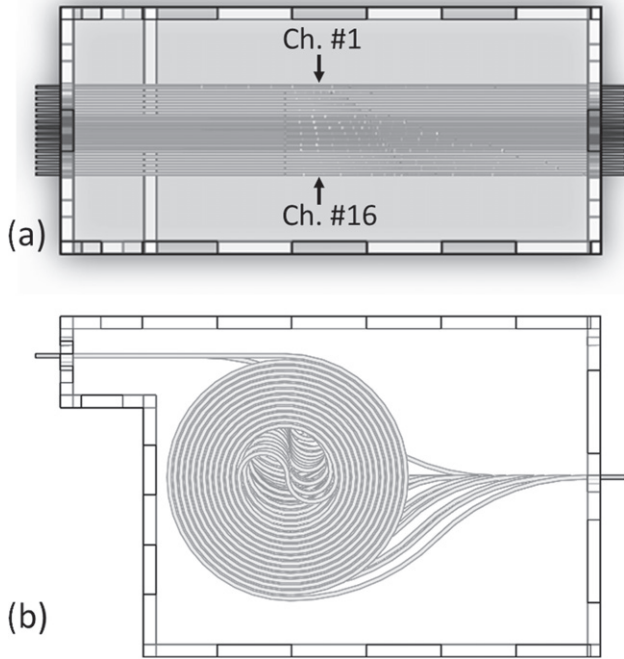


Figure 2. The assembly of 16-channel silicon PADL array (a) top view (b) side view.

center portion of the PADL structure was made larger than 2 mm to ensure high acoustic transmission efficiency by reducing mode conversion at curved sections of the acoustic delay lines.

Figure 2 shows a 3D design of the assembled 16-channel silicon PADL array with one common input port and one common output port. During PA imaging, the input port is in contact with the imaging target, and all 16 channels detect the incoming PA signals simultaneously. The output port is interfaced with a single-element transducer to receive the transmitted PA signals.

2.2. Fabrication and assembly

The silicon PADLs were fabricated on 4 inch {100}-oriented single crystal silicon wafers with a thickness of 250 μm (University Wafers, Boston, MA, USA) by using a micro-fabrication process developed previously [19]. First, a 300 nm thick aluminum layer was deposited on the silicon wafers by electron-beam evaporation. Second, the deposited aluminum layer was patterned with photolithography and wet etching, forming a mask for silicon etching. Third, the silicon PADL structures were directly formed on the silicon wafers by removing unwanted regions with DRIE. In the last step, the etched PADL structures were separated from each other for final assembly.

To precisely position the silicon PADLs in the array at the input and output ports, two identical spacer structures were laser cut from a 0.4 mm thick clear acrylic sheet using the laser engraving and marking machine (PLS6.75, universal Laser Systems, Scottsdale, AZ, USA) (figure 3). Each spacer structure consists of 16 shallow trenches (300 μm \times 500 μm)

to support the silicon PADLs and 15 interspaced deep trenches (200 μm \times 1000 μm) to reduce acoustic crosstalk between adjacent supports. Both the shallow and deep trenches were formed by using a dicing saw. To protect the entire silicon PADL array, an acrylic housing was also fabricated (see figure 2). Its top panel, bottom panel, and two side walls were laser cut from a 1.5 mm thick acrylic sheet.

The assembly process of the silicon PADL array is illustrated in figure 4. First, the bottom panel, side panels, and the two spacers were bonded together with acrylic cement, then the 16 silicon PADLs were placed in the spacer grooves. The PADLs were fastened with two small parts for mechanical stability. In the last step, the top panel was cemented in place to form a sealed housing. The input and output ends were polished to ensure uniform contact with both the imaging target and the ultrasonic transducer. Figure 5 shows the fully assembled 16-channel silicon PADL array.

2.3. The acoustic acceptance angle of silicon PADLs

For PA imaging, the acceptance angle of the detector is an important factor to determine the spatial resolution. Based on the principle of reciprocity, the detection pattern of a detector is the same as its radiation pattern. The silicon PADLs can be treated as a linear array with a small element separation (b) (figure 6(a)). The directivity factor of its far-field radiation pattern in the lateral direction can be estimated by

$$D(\theta) = \frac{\sin((\pi d/\lambda)\sin\theta)}{(\pi d/\lambda)\sin\theta}, \quad (1)$$

where d is the total width of the linear array in the lateral direction, λ is the ultrasound wavelength, and θ is the angle relative to the normal direction of the linear array [21]. Figure 6(b) shows the calculated directivity factor of the 16-channel silicon PADLs (with a total width d of 9 mm) in water at the frequency of 2.25 MHz. The radiation power quickly drops to less than -20 dB when θ reaches 4° , which indicates a small acceptance angle in the lateral direction.

Since all the PADLs have the same detection pattern in the elevational direction, the acceptance angle in the elevational direction the silicon PADLs can be determined with a single delay line from equation (1) (figure 7(a)), where d represents the width (500 μm) of the single delay line. Figure 7(b) shows the calculated directivity factor of single delay line in water at the frequency of 2.25 MHz. The radiation power only drops to -6 dB when θ reaches 55.7° , which indicates a large acceptance angle. This is mainly due to the relatively small element size compared with the ultrasound wavelength in water at 2.25 MHz. To better understand and visualize the radiation pattern, a numerical simulation was conducted to estimate the ultrasound propagation and radiation from single delay line by using Wave 2500[®] (CyberLogic, Inc., New York, NY, USA). Thirty-one virtual ultrasound receivers were used to measure the radiation power at different angles ranging from 0 to 90° (figure 8(a)). The directivity factor of single silicon PADL was determined based on the measured radiation power (figure 8(b)), which matches well with that calculated from equation (1) (figure 7(b)).

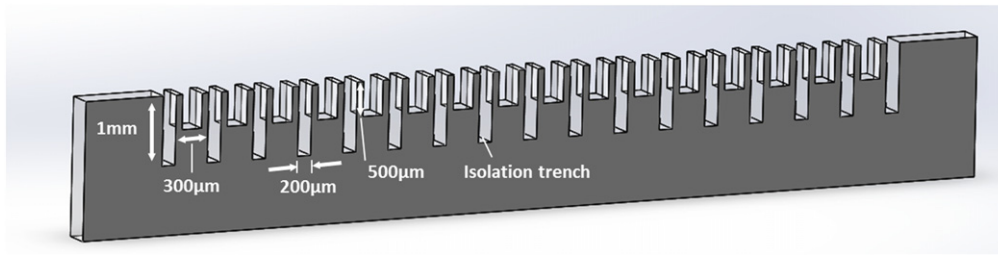


Figure 3. Design for spacers of the input and output port.

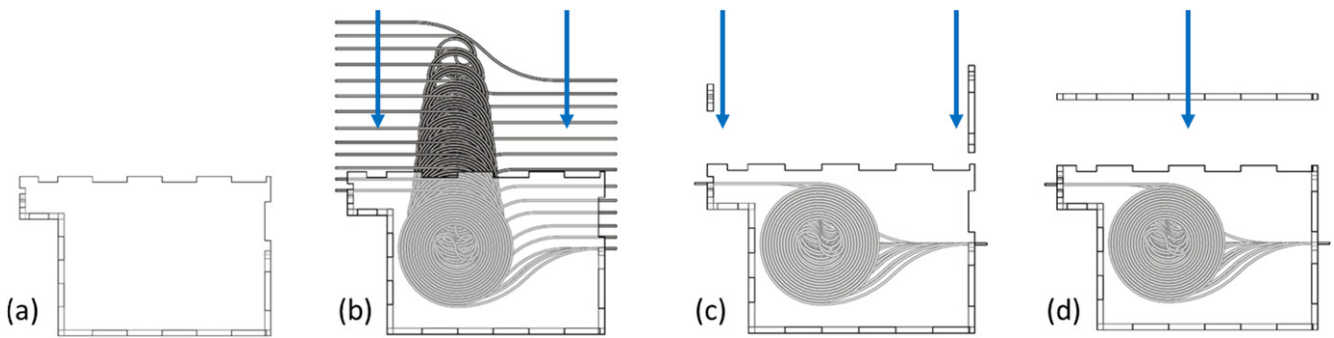


Figure 4. Assembly process of the PADL array. (a) Assembling two sidewalls, bottom, front, back, and spacers. (b) Arranging and placing 16 PADLs. (c) Fastening PADLs (d) affixing top panel.

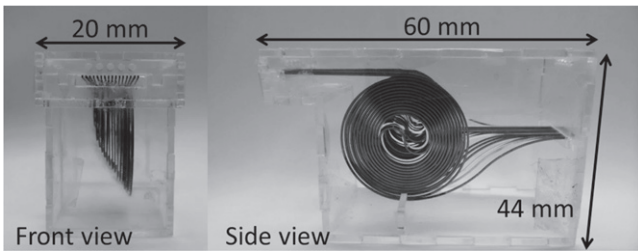


Figure 5. Fully assembled 16-channel silicon PADL array. Reprinted with permission from [15]. Copyright 2015 SPIE.

Olympus NDT, Waltham, MA, USA) were used to transmit and receive the ultrasound signals. The input and output ports of the silicon PADL array were placed in contact with the transmitting and receiving transducers, respectively. Mineral oil was applied between both ends of the silicon PADLs and the surfaces of the transmitting and receiving transducers to enhance the coupling efficiency and minimize unwanted reverberation. The pulser/receiver (5072PR, Olympus NDT, Waltham, MA, USA) was set to transmission mode and sent a driving voltage pulse to the transmitting transducer, which both generated ultrasound signals and also amplified signals detected by the receiving transducer. The ultrasound signals from the transmitting transducer traveled from the input port to the output port through the 16-channel silicon PADLs with distinctly different amounts of time delay. To improve the SNR (signal-to-noise ratio), all 16 channels of ultrasound signals were averaged 16 times and recorded on a digital oscilloscope (TDS2014B, Tektronix Inc., Beaverton, OR, USA).

3. Ultrasonic characterization and PA imaging

3.1. Ultrasonic testing setup

A two-port ultrasound testing setup was built to characterize the acoustic transmission properties of the assembled silicon PADL array (figure 9). Two 2.25 MHz transducers (V104,

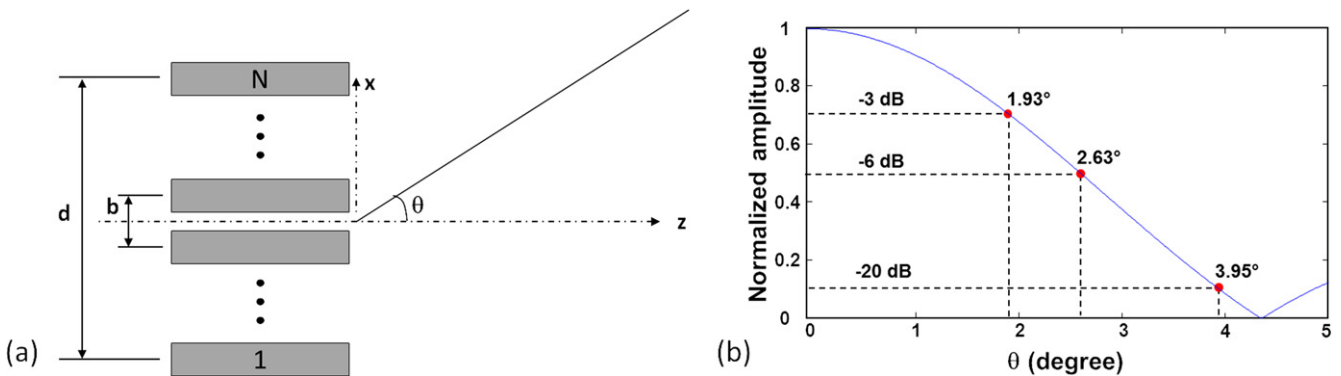


Figure 6. (a) A linear array of PADLs (b) the directivity factor in the lateral direction calculated from equation (1).

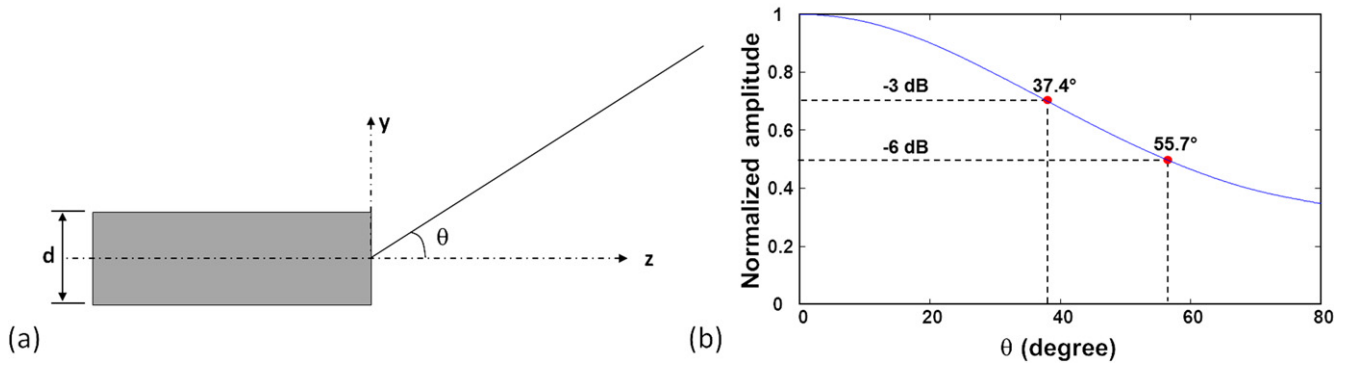


Figure 7. (a) A single PADL (b) the directivity factor in the elevation direction calculated from equation (1).

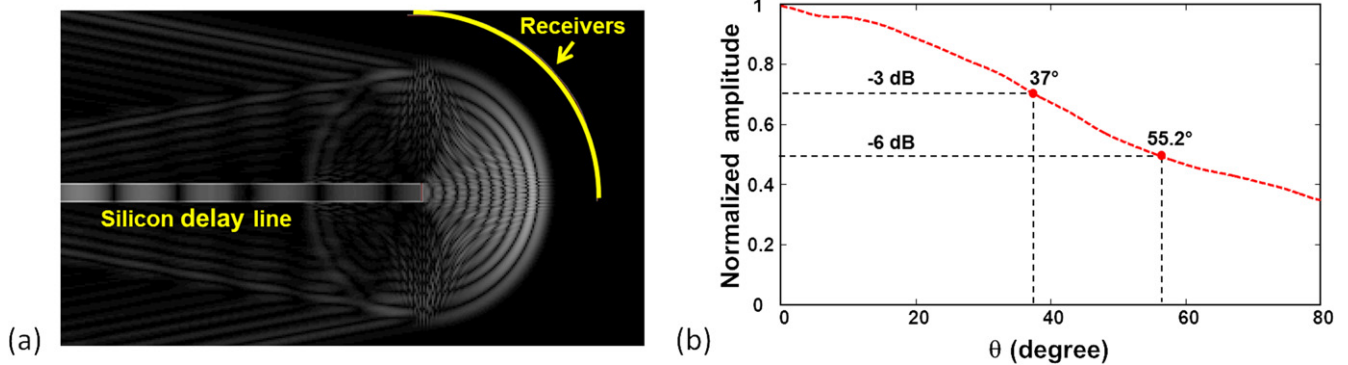


Figure 8. (a) The simulated radiation pattern of single silicon delay line in Wave 2500® (b) the directivity factor estimated from the simulation data.

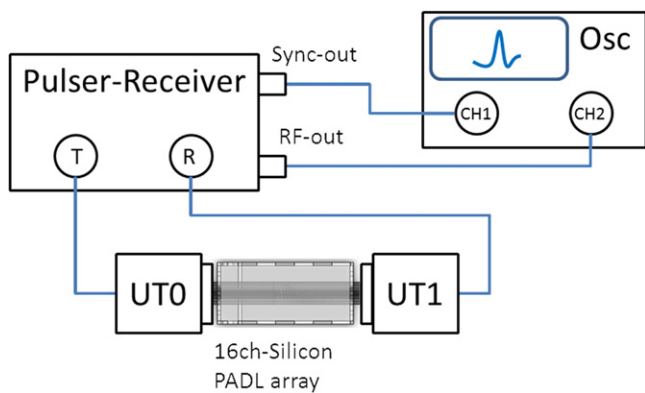


Figure 9. A two-port ultrasound testing setup with the 16-channel silicon PADL array. Osc: Oscilloscope. UT0, UT1: Ultrasonic transducers 0 and 1.

3.2. PA imaging setup

Figure 10 shows the experimental setup of the PA imaging experiment. A frequency-doubled Q-switched 532 nm Nd: YAG laser (LT-P100, Mychway Technology Co., Limited, Shenzhen, Guangdong, China) was the light source. The laser pulse duration was 8 ns and the pulse repetition rate was 5 Hz. The imaging target was a piece of silicon (1 mm × 0.25 mm × 1 mm) embedded in an optical tissue phantom (100 mm × 100 mm × 50 mm). The phantom was composed of 2% agar gelatin by weight, and the target was located 2.5 mm below the phantom surface (figure 12(a)). The

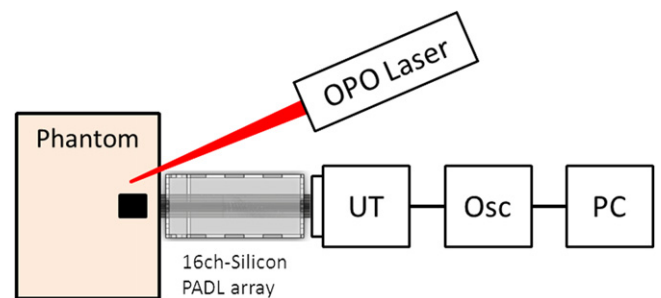


Figure 10. PA imaging setup with the 16-channel silicon PADL array.

PA signals generated from the imaging target propagated along the silicon PADL array and were received by a single-element 2.25 MHz ultrasonic transducer (V106, Olympus NDT, Waltham, MA, USA), then amplified by a pulser/receiver (5072PR, Olympus NDT, Waltham, MA, USA). The amplified PA signals were averaged five times and then recorded on a digital oscilloscope (TDS2014B, Tektronix Inc., Beaverton, OR, USA) at a sampling rate of 5 MHz.

3.3. PA DAQ and image reconstruction

The PA signals were averaged five times to generate one PA image; thus the imaging speed was 1 Hz. The end of each PADL on the sample surface was considered as a single

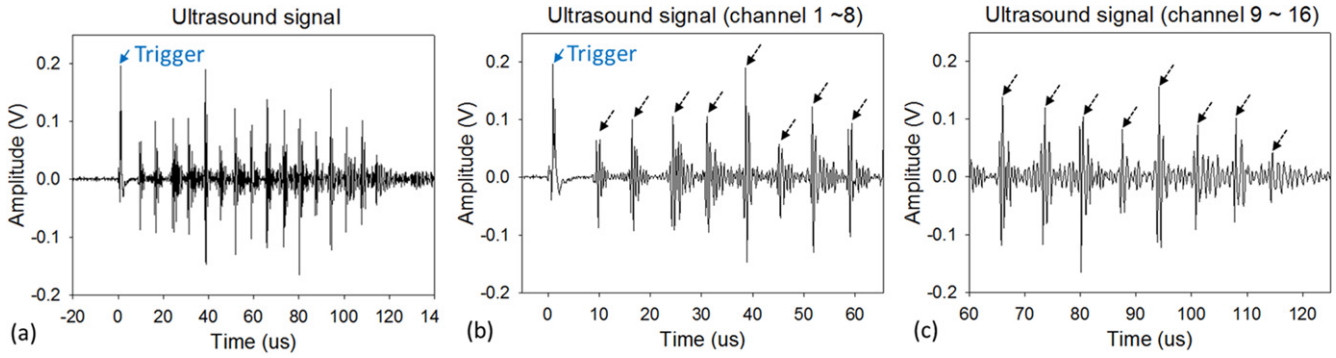


Figure 11. 2.25 MHz ultrasound signals propagating through the 16 silicon PADLs. (a) A trigger and 16 signals. (b) Zoomed-in view of a trigger and the eight signals from channels 1 to 8. (c) Zoomed-in view of the eight signals from channel 9 to 16. Reprinted with permission from [15]. Copyright 2015 SPIE.

element in an ultrasound array. Each sequentially detected PA signal was reshaped into 16 separate PA signals, based on the predefined time positions measured by the ultrasound transmission experiment. To reconstruct PA images, a commonly used delay-and-sum beamforming method was applied [22]. The PA images were reconstructed by summing the data from all 16 channels after compensating for the time delays in each silicon PADL, based on its length and matching phase. In a two-dimensional beam field along the x and z directions, the time delay τ_n for the n th PADL located on (x_n, z_n) can be calculated as follows:

$$\tau_n = \frac{\sqrt{(x - x_n)^2 + (z - z_n)^2} - R}{c}, \quad (2)$$

where R is the distance from the focal point to the center of the delay line, and c is the speed of sound in soft tissue, 1540 m s^{-1} . Envelope detection was applied by using Hilbert transformation along the axial direction (the z direction), followed by taking the absolute value.

4. Results and discussion

4.1. Ultrasonic transmission through the silicon PADL array

Figure 11(a) shows the 16 channels of time-delayed ultrasound signals received by the single-element ultrasonic transducer. The acoustic delay in each ultrasound signal was determined by measuring the time interval between its peak intensity and that of the trigger signal (figures 11(b) and (c)). The average incremental acoustic delay between two adjacent channels was $\sim 7 \mu\text{s}$, slightly longer than designed value of $6.5 \mu\text{s}$. This difference is due to the fact that when they travel in the curved portion of the silicon PADLs, the ultrasound signals encounter multiple reflections on the sidewalls. As a result, their velocity is different from that in a straight line and their actual travel distance is longer than the length of the silicon delay lines. The acoustic attenuation was determined based on the change in the amplitude of the ultrasound signals as they propagated through different distances. Theoretically, acoustic attenuation varies linearly with the length of the silicon PADLs, but the amplitudes of the received ultrasound

signals showed otherwise. One possible reason could be non-uniform contact between the silicon PADLs and the two ultrasound transducers. Here, the average acoustic attenuation of the silicon PADLs was calculated by measuring the signal amplitude difference between the shortest (1st) and the longest (16th) PADL. It was 0.058 dB cm^{-1} @ 2.25 MHz , which is higher than that in a straight silicon delay line (0.015 dB cm^{-1} @ 2.25 MHz) [19]. As observed in our previous experiments [19], when ultrasound signals travel along a curved delay line, they encounter more reflections and potential mode conversions on the sidewall of the delay line, which contribute to higher acoustic attenuation. However, it should be mentioned that the attenuation of 0.058 dB cm^{-1} is still very low, and can be neglected.

4.2. PAT imaging

Figures 12(b)–(d) show the 16 PA signals from the silicon PADL array acquired by the single-element ultrasound transducer and the DAQ channel after five times averaging. Each PA signal was identified based on the time delay ($7 \mu\text{s}$) previously determined in ultrasound transmission testing. Figure 13 shows the reconstructed PA image in Matlab[®]. The envelope of the PA signals was detected by using Hilbert transformation, and the PA image was reconstructed using the synthetic aperture focusing technique [23] to improve spatial resolution. As shown in figure 13(a), in the reconstructed PA image, both the location and the size of the imaging target match the actual values. The image contrast, defined as $(PA_{\text{target}} - PA_{\text{background}})/PA_{\text{background}}$, is calculated to be ~ 1.9 . The spatial resolution, defined as the one-way distance between 10% and 90% of the maximum, divided by the minimum, is $\sim 2.1 \text{ mm}$. Figure 13(b) shows the enhanced PA image after applying a signal threshold of 30%.

5. Conclusion

In this work, we have successfully demonstrated a micro-machined silicon PADL array for real-time PAT. The array capitalizes upon the extremely low acoustic loss of single-crystalline silicon and the high precision of the micromachining

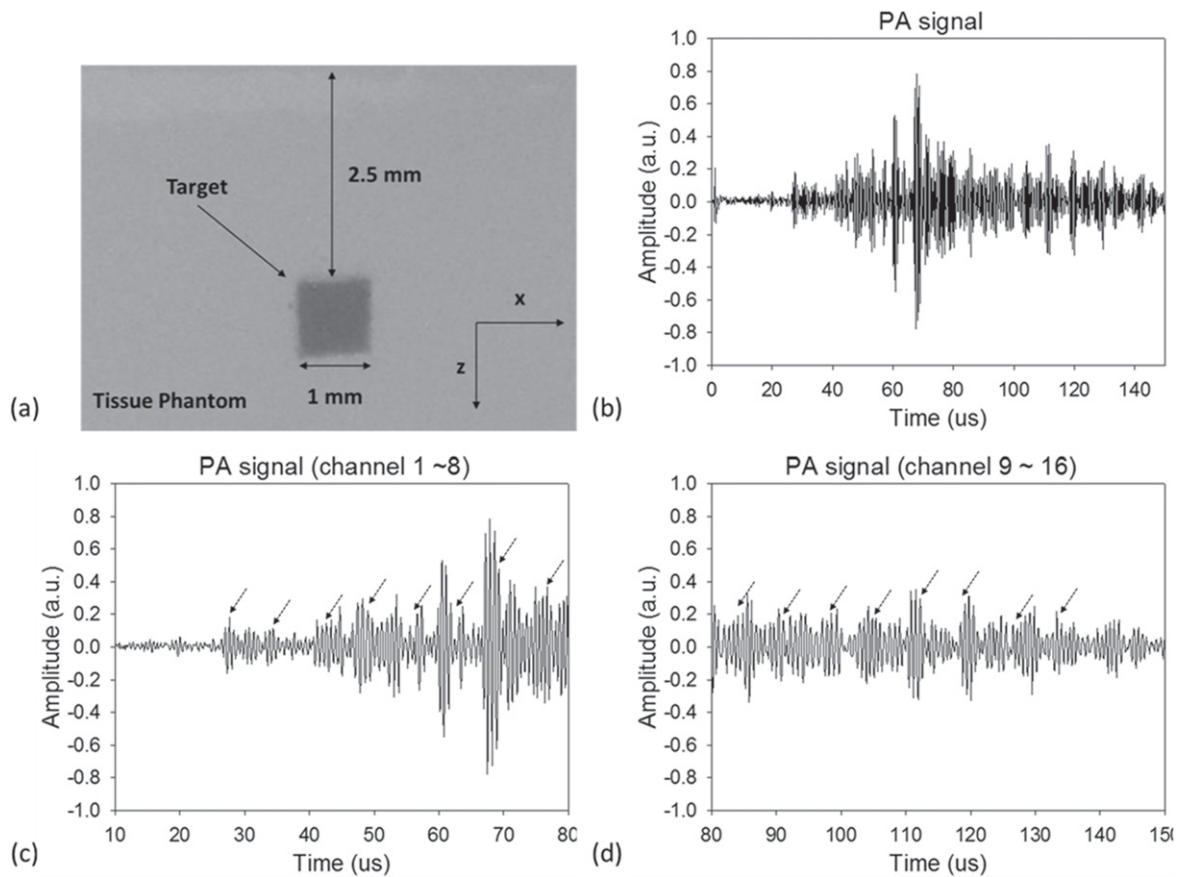


Figure 12. (a) Photography of an optically absorbing target embedded in an optically scattering medium. (b) PA signals received by the ultrasonic transducer through the 16 silicon PADLs. (c) Zoomed-in view of the eight signals from channel 1 to 8. (d) Zoomed-in view of the eight signals from channel 9 to 16. Reprinted with permission from [15]. Copyright 2015 SPIE.

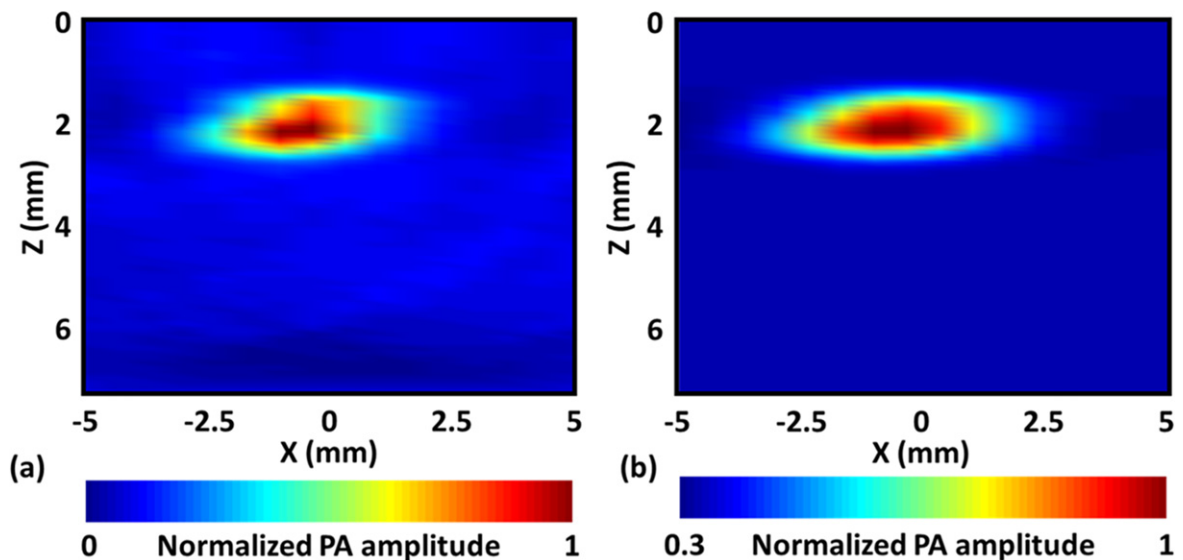


Figure 13. (a) Reconstructed PA image of the imaging target. (b) Thresholded (30%) PA image of (a). Reprinted with permission from [15]. Copyright 2015 SPIE.

process. Using the silicon PADL array, a transducer/channel reduction ratio of 16:1 was achieved, which is twice what was obtained previously with optical-fiber PADLs. In the future, larger silicon PADL arrays will be investigated to provide even higher transducer/channel reduction ratios to fulfill the potential

of the time-delayed ultrasound reception approach. In addition, new solutions will be developed to improve the sensitivity, the acoustic acceptance angle in the elevation direction, and impedance matching at the input terminals to obtain better PA signal detection.

Acknowledgments

This work was supported in part by a grant (CMMI-1131758) from the National Science Foundation to J Zou and a grant (DP1 EB016986) from the National Institutes of Health to L V Wang. Wang has a financial interest in Microphotoacoustics, Inc. and in Endra, Inc., which, however, did not support this work.

References

- [1] Pellacani G, Guitera P, Longo C, Avramidis M, Seidenari S and Menzies S 2007 The impact of *in vivo* reflectance confocal microscopy for the diagnostic accuracy of melanoma and equivocal melanocytic lesions *J. Investigative Dermatology* **127** 2759–65
- [2] Svoboda K and Yasuda R 2006 Principles of two-photon excitation microscopy and its applications to neuroscience *Neuron* **50** 823–39
- [3] Wojtkowski M, Srinivasan V, Fujimoto J G, Ko T, Schuman J S, Kowalczyk A and Duker J S 2005 Three-dimensional retinal imaging with high-speed ultrahigh-resolution optical coherence tomography *Ophthalmology* **112** 1734–46
- [4] Pawley J B 2006 *Handbook of Biological Confocal Microscopy* ed J B Pawley (New York: Springer) pp 20–42
- [5] Theer P and Denk W 2006 On the fundamental imaging-depth limit in two-photon microscopy *J. Opt. Soc. Am. A* **23** 3139–49
- [6] Oraevsky A and Karabutov A 2003 *Biomedical Photonics Handbook* ed T Vo-Dinh (Boca Raton, FL: CRC Press) pp 1–34
- [7] Wang L V 2009 *Photoacoustic Imaging and Spectroscopy* (Boca Raton, FL: CRC Press)
- [8] Kim C, Favazza C and Wang L V 2010 *In vivo* photoacoustic tomography of chemicals: high-resolution functional and molecular optical imaging at new depths *Chem. Rev.* **110** 2756–82
- [9] Wang L V 2009 Multiscale photoacoustic microscopy and computed tomography *Nat. Photonics* **3** 503–9
- [10] Maslov K, Stoica G and Wang L V 2005 *In vivo* dark-field reflection-mode photoacoustic microscopy *Opt. Lett.* **30** 625–7
- [11] Wang X, Pang Y, Ku G, Xie X, Stoica G and Wang L V 2003 Noninvasive laser-induced photoacoustic tomography for structural and functional *in vivo* imaging of the brain *Nat. Biotechnol.* **21** 803–6
- [12] Gamelin J, Maurudis A, Aguirre A, Huang F, Guo P, Wang L V and Zhu Q 2009 A real-time photoacoustic tomography system for small animals *Opt. Express* **17** 10489–98
- [13] Gamelin J, Aguirre A, Maurudis A, Huang F, Castillo D, Wang L V and Zhu Q 2008 Curved array photoacoustic tomographic system for small animal imaging *J. Biomed.* **13** 024007
- [14] Cho Y, Chang C-C, Yu J, Jeon M, Kim C, Wang L V and Zou J 2014 Handheld photoacoustic tomography probe built using optical-fiber parallel acoustic delay lines *J. Biomed. Opt.* **19** 086007
- [15] Cho Y, Chang C-C, Wang L V and Zou J 2015 A micromachined silicon parallel acoustic delay line (PADL) array for real-time photoacoustic tomography (PAT) *SPIE BiOS* (San Francisco, CA: International Society for Optics and Photonics) pp 93232Z–93235Z
- [16] Auld B A 1973 *Acoustic Fields and Waves in Solids* vol 1 (New York: Wiley)
- [17] Yapici M K, Kim C, Chang C-C, Jeon M, Guo Z, Cai X, Zou J and Wang L V 2012 Parallel acoustic delay lines for photoacoustic tomography *J. Biomed. Opt.* **17** 116019
- [18] Cheeke J D N 2012 *Fundamentals and Applications of Ultrasonic Waves* (New York: CRC press)
- [19] Chang C-C, Cho Y, Wang L and Zou J 2013 Micromachined silicon acoustic delay lines for ultrasound applications *J. Micromech. Microeng.* **23** 025006
- [20] Meeker T 1960 Dispersive ultrasonic delay lines using the first longitudinal mode in a strip *IRE Trans. Ultrason. Eng.* **7** 53–8
- [21] Beranek L L and Mellow T 2012 *Acoustics: Sound Fields and Transducers* (Waltham, MA: Academic)
- [22] Xu M and Wang L V 2005 Universal back-projection algorithm for photoacoustic computed tomography *Phys. Rev. E* **71** 016706
- [23] Ylitalo J T and Ermert H 1994 Ultrasound synthetic aperture imaging: monostatic approach *IEEE Trans. Ultrason. Ferroelectr. Freq. Control* **41** 333–9